To appear in *Quantitative InfraRed Thermography*
Vol. 00, No. 00, Month 20XX, 1–15

Fiber orientation assessment in complex shaped parts reinforced with carbon fiber using infrared thermography

H.C. Fernandes[a] * and X. Maldague[a]

[a] *Computer Vision and Systems Laboratory (CVSL), Department of Electrical and Computer Engineering, Laval University, Quebec City, Canada.*

(*Received 00 Month 20XX; final version received 00 Month 20XX*)

The use of composite materials is growing more and more every day in several applications. The arrangement or orientation of the fibers relative to one another have a significant influence on the strength and other properties of fiber reinforced composites. Thus, evaluation techniques are needed for measuring material fiber orientation. In this work infrared thermography is employed to assess the material's fiber orientation. More specifically a pulsed infrared diode laser heating spot technique combined with a 3D model of the part is used in order to assess fiber orientation on the surface of carbon fiber-reinforced polymer (CFRP) complex shaped parts made of carbon/PEEK (*Polyether ether ketone*) randomly-oriented strands (ROS).

Keywords: composite materials; complex shaped parts; fiber orientation; infrared thermography; 3D model

1. Introduction

The use of composite materials (CM) has grown during the past years and this growth will continue in the near future. Today they are widely used in industry. One of the reasons is that their strength and stiffness are comparable to metals with the added advantage of significant weight reduction. Efficient, fast and low-cost manufacturing technologies are required as a large number of structures will be manufactured using composites in the near future. Also, technologies to measure and insure the quality of those manufactured parts are (and will be) in high demand. The arrangement or orientation of the fibers relative to one another, concentration and distribution have a significant influence on the strength and stiffness of fiber reinforced composites. Thus, one needs to develop testing techniques to assess the material's fiber orientation. Destructive methods can be employed to evaluate the fiber on a composite, e.g. cutting a section of the material, polishing the area and evaluating it with microscopy. However, the destructive approach is not always an option since the sample will be damaged after the inspection and probably unfit for use. Thus, Non-Destructive Testing (NDT) techniques must be employed in some cases to assess the material's fiber content.

Infrared Thermography (IT) is a well-known and widely used NDT technique for composite material inspection. In active IT an external heat source is used to stimulate the material being inspected in order to generate a thermal contrast between the feature of interest and the background. The active approach is adopted in many cases given that

*Corresponding author. Email: henrique-coelho.fernandes.1@ulaval.ca

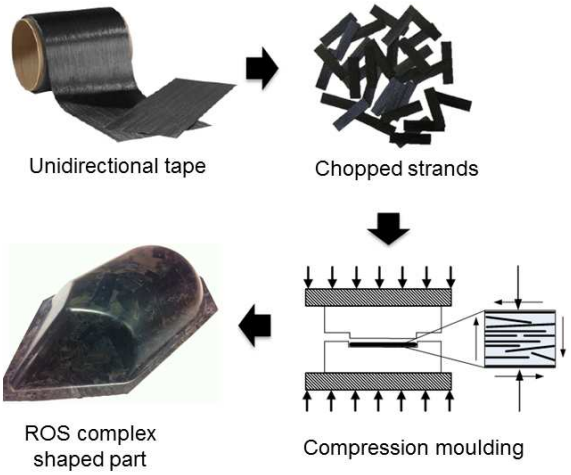

Figure 1. Processing cycle of ROS composite. Size of the strands was 25.4 x 6.35 mm prior to moulding.

the inspected parts are usually in equilibrium with the surroundings [1]. Qualitative and quantitative assessment of flaws is a very popular application of IT for CM. However there are others such as fiber orientation assessment. In this paper active IT is used in order to assess fiber orientation on the surface of carbon fiber-reinforced polymer (CFRP) complex shaped parts made of carbon/PEEK (*Polyether ether ketone*) random-oriented strands (ROS). A 'laser spot' technique, referred to here as Pulsed Thermal Ellipsometry (PTE), is used to locally measure the material's fiber orientation. In the case of fiber reinforced composites, which are thermally anisotropic, the thermal pattern formed on the surface of the material due to the thermal stimulation is an ellipse where its major axis orientation is related to the fiber orientation.

Figure 1 shows the part tested in this paper (with curvatures, edges and corners) in its manufacturing cycle. In the case of ROS parts, fiber orientation on the surface is random since each strand has its own fiber orientation. The size of the strands was 25.4 x 6.35 mm prior to moulding. Due to this ROS characteristic, several strands (located in different regions) were tested using PTE. For a more accurate quantitative result, mapping of infrared data onto a 3D model of the scanned part (or dense 3D point cloud) was applied to aide in the correct quantitative interpretation of the thermal pattern on the part's surface and as a consequence accurate fiber orientation measurements. It is worth mentioning here that only one camera was used and it was kept motionless during all tests (i.e. the scene view and camera's angle of incidence did not change according to the tested region and where the region was on the part's surface).

This paper is organized as follows: the next section presents a brief literature review on IT for fiber orientation assessment (PTE); in Sec. 3 the used 3D approach is described; in Sec. 4, experiments and results are presented and our final considerations are presented in Sec. 5.

2. Pulsed Thermal Ellipsometry

More than one century ago, De Senarmont [2] applied a thermal approach to determine the principal orientations in crystal plates: he covered them with a thin layer of wax, heated them over a small spot and monitored the isotherm shape revealed by the solid/liquid transition contour appearing in the wax layer. The isotherm proved to be elliptical and its aspect ratio related to the square root of the principal conductivities in the surface plane.

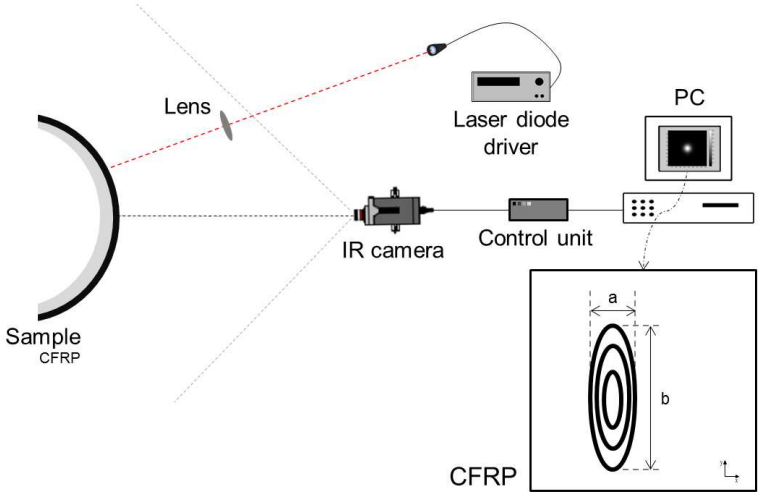

Figure 2. Pulsed Thermal Ellipsometry (PTE) schematic set-up for fiber orientation assessment in CFRP.

This method, referred to by Krapez et al. [3–6] as Thermal Ellipsometry, was later used for various applications (with, of course, up-to-date experimental equipment) by means of thermography. It was applied on polymer materials to establish a correlation between their draw ratio and the induced thermal anisotropy. It was also used to evaluate the fiber orientation in the case of composite materials using short or long carbon fibers. For the latter problem, authors such as Aindow et al. [7] and Cielo et al. [8] showed that heat propagates faster in the longitudinal direction of fiber on the surface of fiber reinforced laminates. Aindow et al. [7] detected local anisotropy in carbon fiber-reinforced plastic (CFRP - nylon-66) injection mouldings using two methods: thermography using infrared scanning, which reveals anisotropy of thermal conductivity, and polarized shear-wave ultrasonic showing elastic anisotropy. For the thermographic method, they recorded isotherms formed around a heat point source on a plane surface using an infrared imaging camera. The isotherms that they observed were ellipses of which the ratio of lengths of the principal axes (b/a) are proportional to the square root of the ratio of thermal conductivities. They assumed that the longest dimension of the counter in each picture indicated the major axis of thermal conductivity in the surface, which in turn is related to the direction of fiber orientation.

Cielo et al. prepared a review [8] of a number of optical techniques for the characterization of non-metallic materials. One of them was the evaluation of phase (or fiber) orientation in stretched polymer films or in composites by an analysis of the thermal propagation pattern. A typical configuration is shown in Figure 2. They spot-heated the inspected part by a narrow laser beam and the resulting heat-propagation pattern was recorded by an IR camera. If the material is oriented, such as the unidirectional graphite-epoxy sheet they inspected, an elliptical thermal pattern is observed, with the ratio between the two principal axes (b/a) being related to the square root of the thermal conductivities in the longitudinal and transverse directions. A test on an isotropic material would give a circle instead of an ellipse. They illustrated this approach showing results from two 8-ply unidirectional Narmco 5217 sheets which were spot heated for a period of 20 seconds by a laser beam of 0.5 W.

A more detailed theoretical analysis was later undertaken by Krapez [3] through an analytical treatment of thermal diffusion in laminates composed of orthotropic layers assuming the surface is submitted to concentrated heating. Three temporal regimes were considered in that study: steady-state regime, transient regime (as obtained during step heating), and modulated regime (in order to analyze how thermal waves ‘propagate’ in

orthotropic laminates). Experiments were performed on carbon-epoxy laminates for all three regimes. Later, Krapez [4] used the same theory (thermal anisotropy measurements method which consists in analyzing the shape of the isotherms which develop around a heated spot) to develop a thermal inversion method to infer thickness of skin and core layers of a 3-layer carbon/epoxy laminate.

In our previous work [9], as in Karpen et al. [10], lock-in thermography (harmonic thermal waves) is used to probe orientation fields of carbon fibers both along the surface and in depth at low modulation frequencies and within a short time. Later Karpen et al. [11] developed a theoretical model in order to correctly interpret their measurements.

The experimental set-up used during this work was the one shown in Figure 2. The angle of incidence of the laser beam on the plate's surface is always parallel to the normal to the surface, i.e. perpendicular to the surface. With this restriction it is ensured that the the original shape of the heat spot was as close as it could be to a circle. The case where laser beam angle of incidence on the plate's surface is not 0° was studied in our previous work [12]. It is clear that if the angle of incidence is greater than 0°, the initial shape of the excitation point on the plate's surface would not be a circle but an ellipsoid and it would distort the evaluation method. In [12] tests were performed with a laminate with known fiber orientation ($[0^\circ/90^\circ]_{12}$) and it was shown that only laser beam angles of incidence greater than $\pm 45^\circ$ will prevent the application of the PTE technique. With angles of incidence less than $\pm 45^\circ$ the technique is still feasible and fiber orientation measurements would be just a couple of degrees off.

Since the goal of this work is to measure fiber orientation just on the surface of complex shaped parts, one image of a specific time of the PTE infrared sequence is used to assess the fiber orientation. If one chooses a very early time, the heat would not have diffused yet on the surface. On the other hand, if one chooses a very late time, the heat would have diffused not only laterally but also in depth. This depth diffusion would generate a thermal response of fiber orientations of deeper layers and the thermal pattern on the surface of the plate would have more information than just the fiber orientation of the surface which is not the goal here. Since we are interested just on the fiber orientation on the surface, an optimal diffusion time should be estimated and the particular image of this optimal diffusion time used for fiber orientation assessment. In this work this estimation is done by an experienced human operator based on the visualization of several experiments. The diffusion time used to select the infrared image in this work is 0.26 seconds.

3. Fusion of infrared and 3D data

The thermal pattern produced due to the heating spot applied on the part is formed on its surface. Since the inspected part has a complex shape and not a flat surface, quantitative interpretation of the thermal pattern on the part's surface will be distorted (assuming that the camera's angle of incidence on the spot is other than 0°) if done directly from the raw 2D image since it is not possible to retrieve depth information from the 2D image (at least directly). The surface point temperature information would be projected on a 2D plane and the geometry information of the 3D surface would be lost. Consequently, the resulting outcome of the thermal pattern interpretation would be an erroneous measurement of the fiber orientation direction of that spot on the surface. To overcome this problem, a 3D model of the part is used together with the thermal image to ensure a correct quantitative analysis of the thermal pattern, which is an ellipse in the case of CFRP, and consequently a correct measure of the fiber orientation on the surface.

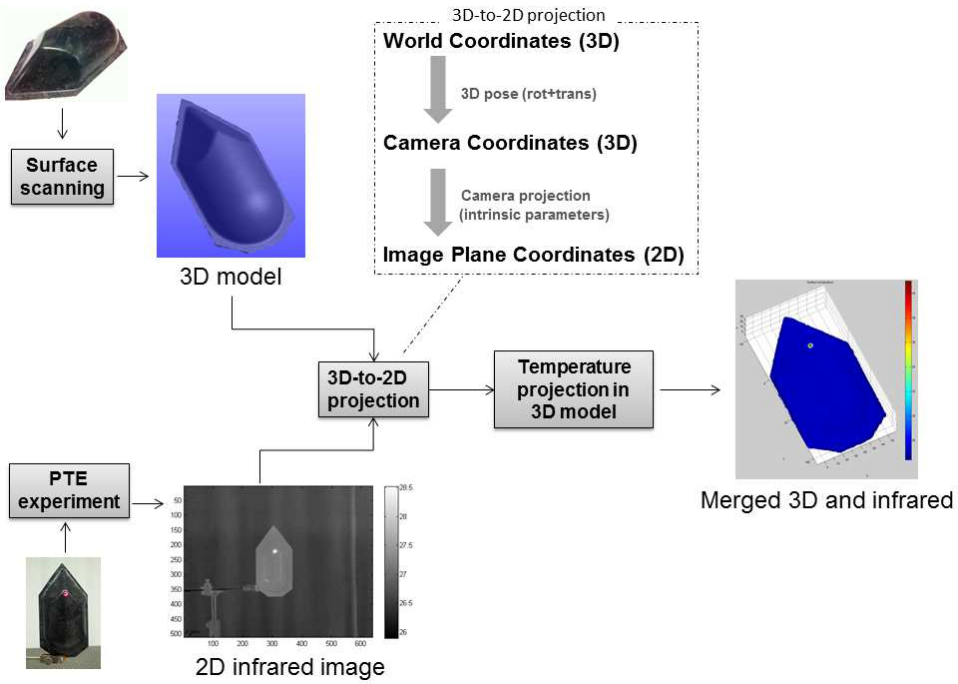

Figure 3. Steps of the fusion process of infrared and 3D data.

The thermal information provided by the infrared camera is combined with a 3D model of the surface of the part (or a 3D dense point cloud) which is obtained by previously scanning the part. The merge of these two pieces of information (infrared and 3D) allows the correct quantitative analysis of the elliptical pattern overcoming the problem of losing the surface's geometric information and also the case where the camera does not have a frontal view of the inspected area (i.e. when the camera's angle of incidence is other than 0°).

Figure 3 summarizes the basic steps necessary to fuse the infrared and 3D data. The output of this merge is a 3D thermal image. One can uses a temperature threshold to extract the ellipse from the merged image and then calculate its orientation. This section presents how the 3D data is combined with the 2D infrared image and how the fiber orientation is extracted from the merged 3D thermal image.

3.1. *Capturing the 3D model of the part*

In order to capture the 3D shape of objects, a commercially available 3D scanner ($CreaformGo!SCAN®$ [13]) has been used. In contrast to laser scanners, the scanner and the software ($CreaformVXelements®$) allow the user to build a complete 3D model of an object by automatically combining multiple measurements. The handheld scanner has to be manually moved around the object to do this. The scanner is geometrically calibrated and reports the object dimensions in millimeters. The model resolution can be as small as 0.5 mm. The software guides the user during acquisition and post-processing of the data. It offers post-processing functionalities such as surface reconstruction/optimization, hole filling and artifact removal. Also, features of interest can be introduced: points, lines, planes and surface can be fitted in the model. Points of interest previously selected are added to the model to be used in the next steps of the 3D/infrared merging process. By default the center of the used coordinate system is the position and orientation of the scanner in the first scan. However the software provides

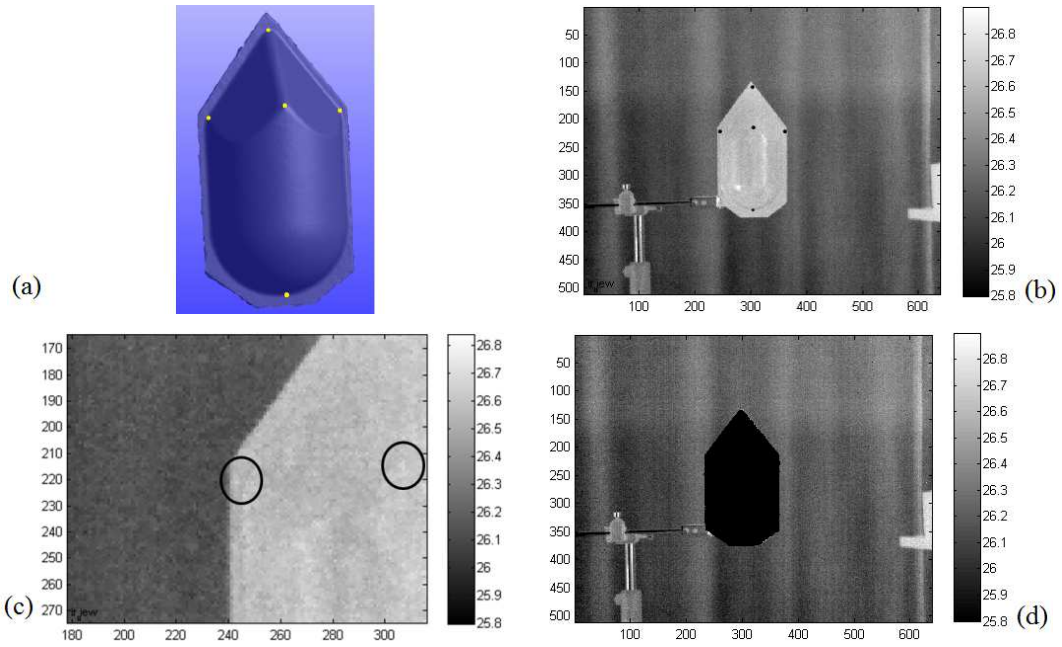

Figure 4. (a) 3D generated model with five selected points shown. (b) 2D infrared image. Dark points were added to the image to indicate the location of the same five selected before. (c) Enlarged 2D infrared image focusing on two selected feature points. (d) 2D infrared image with re-projected black points corresponding of the calculated x-y position of each point of the 3D model.

options to change the coordinate system and align it with points, planes or lines in the 3D model. The generated mesh, with all its added features, can be exported in various ASCII and binary standard formats. The exported data is imported into $Matlab^{®}$ to perform the next steps of the 3D/infrared fusion. After the process of scanning, hole filling and feature adding is completed, a set of points of the form $P_{wi}\,(X_{wi}, Y_{wi}, Z_{wi})$ is generated that corresponds to the part's 3D model where $i \in [1, \ldots, N]$.

Figure 4(a) shows the final 3D model generated with the $CreaformVXelements^{®}$ software with five selected points which are going to be used to find the 3D pose of the object in the infrared image. Figure 4(b) shows the infrared 2D image (a 640 x 512 image recorded with a Indigo Phoenix Thermal Camera from FLIR Systems©) with added dark points which correspond to the positions of the points selected before in the 3D model. The location of these points is a critical issue. It is important that their locations are as accurate as possible in the two cases (3D model and 2D infrared image) for the next steps of the algorithm. To facilitate the selection of such points in the 2D infrared image, easy selectable positions were chosen such as edges and corners. Figure 4(c) shows an enlarged region of the 2D infrared image containing the position of two feature points. The region where these points should be are circled and the center of these circles correspond to the position of the points. As it can be seen, there is very little contrast in the raw infrared image which makes it difficult to select the points in the same location as they were in the 3D model. To ensure the correct selection of the points positions in the 2D infrared image they were carefully and manually selected based on the distinguishable features of the inspected part, i.e. the edges and corners of the part. If after applying the 3D pose algorithm the position result of the re-projected 3D model points on the raw infrared image were not coherent, a more carefully selection of the five points positions in the 2D infrared image was done again and the algorithm reapplied. This process was repeated until the positions of the re-projected 3D model points were on the part's area in the 2D infrared image (an area which can be easily distinguished from the background as it can be seen comparing Figure 4(b) and Figure 4(d)). The situation where the re-projected

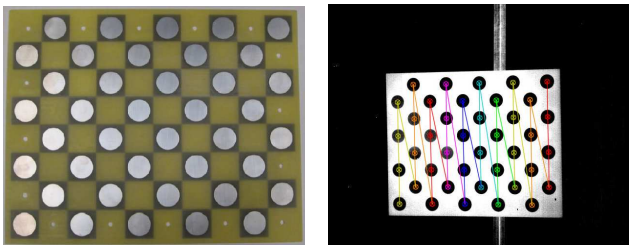

(a) (b)

Figure 5. (a) Calibration target viewed in the visible spectrum, (b) Calibration target seen in the infrared spectrum with the detected features.

points are well placed due to the correct selection of the feature points positions is shown in Figure 4(d). Figure 4(d) shows the same infrared image showed in Figure 4(b) however now the calculated position of each point of the 3D model is marked with a dark point superimposing the original pixels of the infrared image.

3.2. *Infrared camera calibration*

In order to correctly merge the 3D and infrared information, it is important to know the camera parameters (or intrinsic parameters). To determine these parameters one needs to perform a camera calibration. The calibration process consists in identifying the internal quantities of the camera that affect the imaging process: image center position (in pixels), focal length, different scaling factors for row pixels and column pixels, skew factor and lens distortion. These parameters describe the relationship of the camera model coordinate system and the image plane coordinate system [14]. During the calibration process, the camera observes a set of features such as points or lines with known positions in some fixed world coordinate system. In this context, camera calibration can be modeled as an optimization process, where the discrepancy between the observed image features and their theoretical position is minimized with respect to the camera's intrinsic parameters.

A target with circle patterns is used in this project (similar to the ones found in [15, 16]). Features in the target must be seen by the infrared camera thus before image acquisition, the target is heated so the circles can be detected. Figure 5 shows the calibration target and the features detected during the calibration process in the infrared image. Several packages are available, already implemented e.g. in *OpenCV*© or in *Matlab*® [17], to perform this task. Camera pixels are assumed to be square so scaling factors for row and column pixels are neglected as well as the skew factor. The other intrinsic parameters, focal length, image center and lens distortion, are stored and used in the camera perspective projection step.

3.3. *From 3D world coordinates to 2D image pixel coordinates*

3.3.1. 3D pose

The next step required to combine the 3D model and the infrared image is finding the object's 3D pose. It consists in identifying a rotation and translation matrix (R and T respectively) that maps 3D world points (in a 3D model reference system) in 3D camera points (in the camera reference system). A popular algorithm called 'pose from orthography and scaling with iterations' (POSIT) [18] is used. It is a fast iterative algorithm for determining the pose (rotation and translation) of an object or scene with respect to a camera when points of the object are given in some object coordinate system

and these points are visible/recognizable in the camera image, so that corresponding image points and object points can be listed in the same order. POSIT requires at least four points to be recognized in the 3D model and in the 2D image. The algorithm's input points in our experiments were the points shown in Figure 4. Implementation of POSIT can be found online in the author's webpage [19]. In our experiments, the algorithm determines rotation and translation matrices after three iterations.

The transformation from world coordinates (3D model reference system) to camera coordinates can be written as [14]:

$$\begin{bmatrix} X_c \\ Y_c \\ Z_c \\ 1 \end{bmatrix} = \begin{bmatrix} R & T \\ 0 & 1 \end{bmatrix} \times \begin{bmatrix} X_w \\ Y_w \\ Z_w \\ 1 \end{bmatrix} \tag{1}$$

where $P_w\,(X_w, Y_w, Z_w, 1)$ is the point in homogeneous coordinates in the world reference system, $P_c\,(X_c, Y_c, Z_c, 1)$ is the point in homogeneous coordinates in the camera reference system, R is a 3x3 rotation matrix and T a 3x1 translation matrix.

3.3.2. Camera perspective projection

After finding the 3D point coordinate in the camera's reference system by applying the rotation and translation calculated with the POSIT algorithm, the object must be projected onto the image plane in order to determine the correspondence between the 3D points and the pixels in the infrared 2D image. The coordinates $[u, v]$ of the pixels p in the infrared image are given by [14]:

$$\begin{cases} u = \frac{X'}{Z'} \\ v = \frac{Y'}{Z'} \end{cases} \tag{2}$$

where:

$$\begin{bmatrix} X' \\ Y' \\ Z' \end{bmatrix} = \begin{bmatrix} f & 0 & c_x & 0 \\ 0 & f & c_y & 0 \\ 0 & 0 & 1 & 0 \end{bmatrix} \times \begin{bmatrix} X_c \\ Y_c \\ Z_c \\ 1 \end{bmatrix}, \tag{3}$$

f is the camera focal length and $[c_x, c_y]$ the coordinates of the image center position in pixel coordinates.

At the end of this process, a relation is created between each of the $P_{wi}\,(X_{wi}, Y_{wi}, Z_{wi})$ points of the 3D model and one pixel $p\,(u, v) = T$ of the infrared image where T is the temperature value of the pixel. Therefore, the temperature value of a point i of the 3D model is known and for each point of the 3D model a quadruple is created of the form:

$$P_{Ti} = (X_i, Y_i, Z_i, T_i) \tag{4}$$

where $i \in [1, \ldots, N]$; X_i, Y_i and Z_i are its 3D coordinates and T_i is the point's temperature value. Thus, quantitative measurements are done on the set of P_{Ti} points in order to assess the fiber orientation of a heated spot on the surface of the complex shaped part.

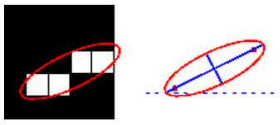

Figure 6. Small binary image and how its orientation is calculated.[20]

3.4. *Ellipse segmentation*

Once the set of P_T points is calculated, the thermal pattern segmentation is performed by a basic thresholding process. The result is an elliptical form from which one can extract its major axis orientation. The ellipse is formed by M points where M is much smaller than N. The ellipse image is a binary image which obeys the following function of belongingness:

$$fbe(P_{Ti}) = \begin{cases} 1, & \text{if } T_i \geq Th \\ 0, & \text{otherwise} \end{cases} \tag{5}$$

where $i \in [1, \ldots, N]$ and Th is the temperature threshold value determined experimentally by an experienced operator after the observation of several experiments. In our experiments Th is usually 28.95°C.

With the resulting binary image, which is represented by a binary matrix, $Matlab^{®}$ native function *regionprops* was used to calculate the ellipse orientation. The orientation of the image, here the ellipse, is the angle (in degrees ranging from $-90°$ to $90°$) between the x-axis and the major axis of the ellipse that has the same second-moments as the region. Figure 6 illustrates the axes and orientation of the ellipse. The left side of the figure shows an image region and its corresponding ellipse. The right side shows the same ellipse with its major and minor axes. The orientation is the angle between the horizontal dotted line and the major axis.

4. Experiments and Results

The experimental set-up used was the same depicted in Figure 2. A Indigo Phoenix Thermal Camera from FLIR Systems©, a $InSb$ cooled camera which operates in the 3.0 - 5.0 μm spectral bandwidth, was used during the experiments. The 2D infrared image spatial resolution was 640 x 512 pixels and the rectangular region covered on the image frame by the tested part was 125 x 200 pixels large which corresponds to the part's maximum width and length respectively (8.4 x 16.4 cm in the real world). The distance from the camera to the plate's closest surface was 139 cm and the camera frame rate was 56 frames per second. Experimental parameters such as heating power and pulse duration were maintained constant during all tests. These parameters are listed in Table 1 and carbon/PEEK thermal properties can be found in [21].

Seven specific points were chosen strategically on different regions on the part's surface to test the proposed solution. Points on strands with different fiber orientation were considered, i.e. how the strand was oriented after the part was moulded and consolidated. The surface geometric nature where the strand was located was also considered, i.e. whether the strand was situated on a spherical surface, on a cylindrical surface, on an edge between a curve and flat surface, on a flat surface (but with a camera's angle of incidence greater than 0°) or on a corner (a region where three different surfaces meet). The locations of the seven selected points are shown in Figure 7.

For each one of the test points, the position of the infrared camera did not change (it

Figure 7. Tested points on the part's surface. Part's size is $8.4x16.4cm$ in the real world.

was neither rotated nor translated). Thus, the heating source had to be moved. For each test, the laser's optic fiber was repositioned so the desired point on the part could be heated. Nevertheless, the angle of incidence of the laser beam on the plate's surface was always parallel to the normal to the surface, i.e. perpendicular to the surface. With this last restriction it was ensured that the the original shape of the heat spot was as close as it could be to a circle.

Another factor considered during the selection of the points to be tested was that the angle of incidence of the camera should not be greater than $\pm 60°$ (i.e. the angle between the camera optical axis and the normal to the point should be less than $\pm 60°$ [12]). This last factor was also considered so that the quantitative analysis could be done with just one 2D infrared image (i.e. just one view). As mentioned before, the pattern formed on the plate's surface is elliptical in anisotropic materials, which is the case of carbon/PEEK composites and the ellipse's major axis orientation is the same as the fiber orientation around that spot.

The PTE technique was then applied on each one of the seven selected points and the heating and cooling down process were recorded. For each PTE test, the approach described in Subsections 3.3 and 3.4 was conducted. Thus, at the beginning of the process a 3D dense point cloud of the part's surface was calculated (performed once) and for each experiment a merge was performed with the infrared information and the 3D dense point cloud. Based on the surface temperature distribution on the 3D part model an elliptical pattern was identified using Equation 5. The fiber orientation associated with

Table 1. Parameters used during experiments.

Parameters	**Value**
Diode-laser frequency	805 nm
Beam power used	5 W of 30 W
Shooting duration	0.1 seconds
Spot diameter on plate's surface	$\sim$ 3 mm
Recording time	10 seconds
Image used to extract fiber orientation	0.26 seconds[a]

[a]After beam had stopped.

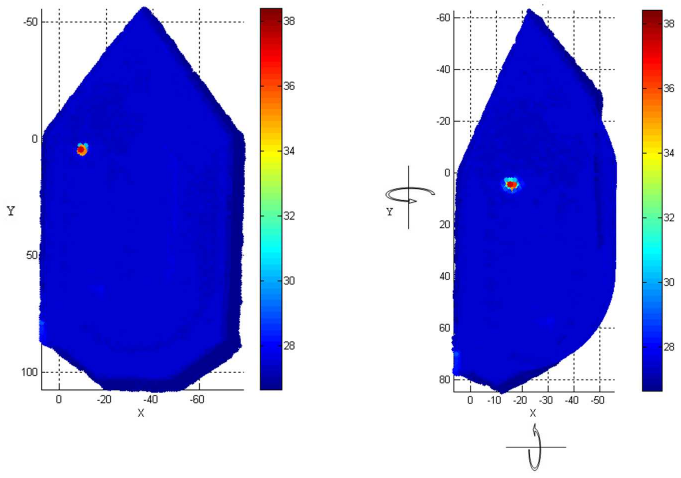

(a) (b)

Figure 8. 3D model camera view rotation. Tested point E temperature values are used as illustration. (a) 3D model before camera view rotation; (b) 3D model after rotation around y-axis followed by a rotation around x-axis.

the tested point was later calculated based on the elliptical pattern from each merge. In order to perform this calculation, each 3D point cloud was rotated around axes x and/or y to ensure that the normal to the point was parallel to the angle of incidence of a virtual camera at an optimized position for the particular test point. In other words, to calculate the ellipse orientation, the model was rotated so that the thermal pattern could be quantified as it was on a flat surface. In Figure 8 it is illustrated for the test point E how the model was rotated. Figure 8(a) shows the model before the rotations and Figure 8(b) shows the model after the rotations around axes y and x were applied. In this case a rotation of 49° around y-axis was applied followed by 30° rotation around x-axis.

Figure 9 shows the results for the seven tested points. The images show the elliptical thermal pattern around the selected test points (A-G) as observed by an ideal infrared camera with optimized axis orientation. The surrounding was suppressed due to application of Equation 5 and the points are plotted with their original temperature values. The white line indicates the ellipse's major axis whose orientation is, as discussed before, the same as the fiber orientation on that particular region. The x-axis is used as reference axis to report the ellipse's major axis orientation. Table 2 shows the ellipse's major axis orientation for each one of the seven tested points.

Figure 10 shows the fiber orientation quantification using only 2D infrared images from

Table 2. Fiber orientation of tested points.

Point	**Fiber orientation**[b]
A	52°
B	44°
C	70°
D	−58°
E	−17°
F	40°
G	25°

[b]Angle between ellipse's major axis and x-axis.

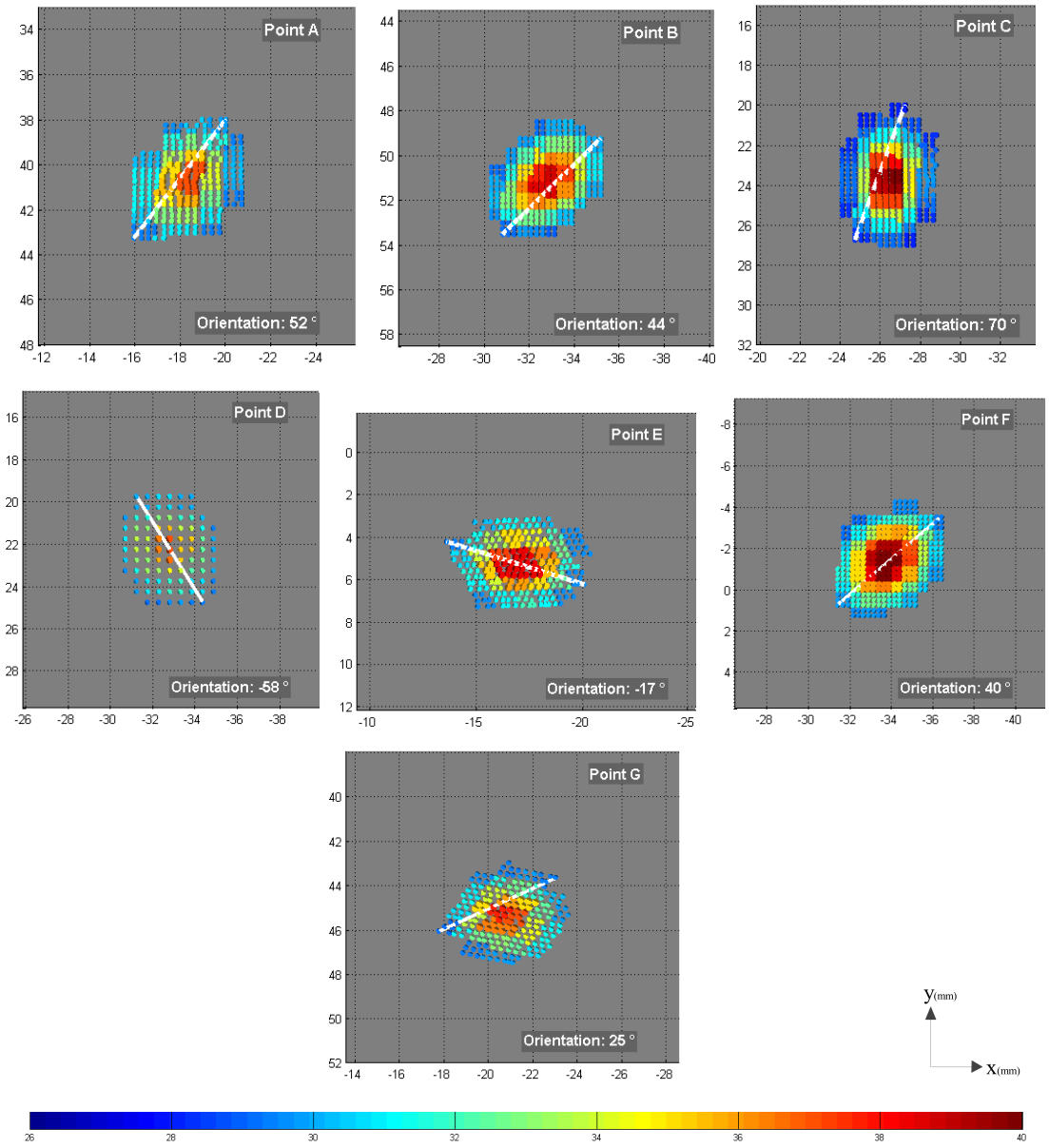

Figure 9. The images show the elliptical thermal pattern around the selected test points (A to G) as observed by an ideal infrared camera with optimized axis orientation. The surrounding was suppressed due to application of Equation 5. The ellipse orientation is the angle between axis x and the white line (the major axis of the ellipse).

PTE experiments and quantifications using the proposed technique. Figure 10(a) shows the elliptical thermal pattern around point E calculated using the 3D/infrared merge approach while Figure 10(b) shows the elliptical thermal pattern around the same point extract when one uses only the 2D infrared information. Figure 10(c) shows the elliptical thermal pattern around point G calculated using the 3D/infrared merge approach while Figure 10(d) shows the elliptical thermal pattern around the same point extract when one uses only the 2D infrared information. The ellipse orientation is the angle between axis x and the white line (the major axis of the ellipse). The orientation is completely different due to the depth effect introduced by the complex shape of the part when using only 2D information. When the 3D and thermal data are analysed together, the correct fiber orientation quantification is achieved. An observation of the part's visible image (Figure 7) and a careful analysis of the spot that was tested (indicated by the white point),

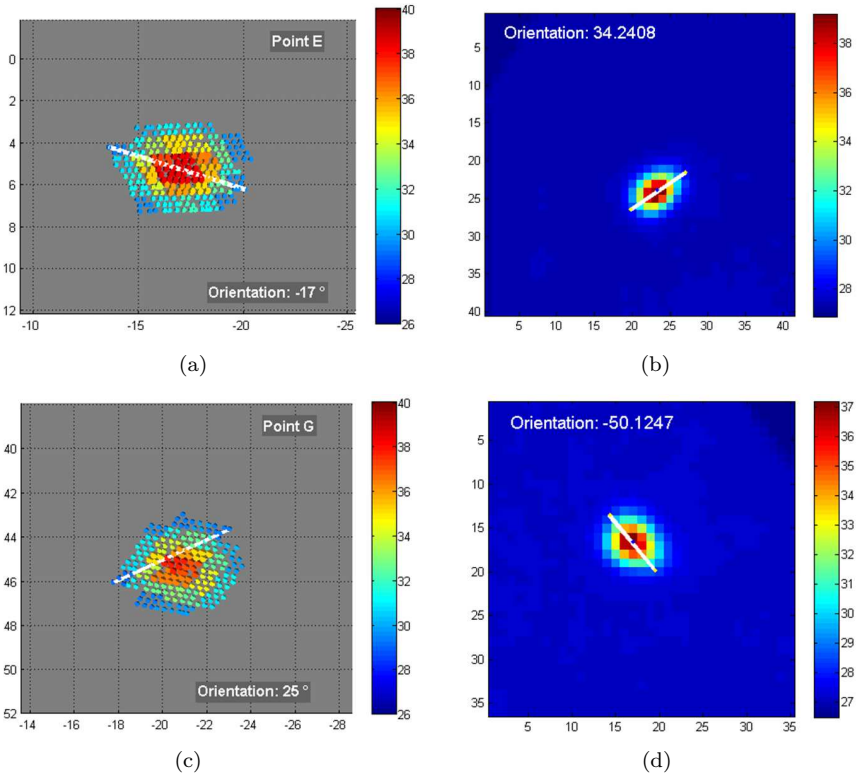

Figure 10. Ellipse major axis: comparison between results obtained using the proposed approach and using only 2D infrared information. (a) Orientation calculated around point E using the 3D/thermal merge process and (b) orientation calculated around the same point E but using just 2D infrared information. (c) Orientation calculated around point G using the 3D/thermal merge process and (d) orientation calculated around the same point G but using just 2D infrared information. The difference in the ellipse's major axis orientation is clearly observed when using fusion of the 3D information and the 2D infrared image and when using only the 2D infrared image.

reveals that the position/orientation of the strand indicates that the fiber orientation is in fact in the direction which was determined using the 3D information rather than the orientation calculated using only the 2D images. This shows how important it is to analyse not only the thermal information but also the 3D information when testing complex shaped parts.

To the naked eye, the fiber orientation of the tested regions is in very good agreement with the orientations measured with the technique. A direct comparison of how fibers are placed on the surface and the results reported in Table 2 was not done because of the randomness nature of the fibers in this kind of plate (ROS) and also because there are some regions where fiber and matrix are deformed/mixed together due to heat and pressure applied during the mould process. A comparison of orientation measured by the technique and the real orientation was performed on a flat laminate with known layup $[0°/90°]_{12}$ in [9, 12]. It was shown in these previous works that PTE is a feasible technique for measuring fiber orientation of carbon/PEEK composites.

5. Conclusions

In this paper an infrared thermography technique using a diode-laser to measure fiber orientation of CFRP was presented. Pulsed Thermal Ellipsometry (PTE) was applied to a complex shaped part and combined with a 3D model of the part's surface in order to conduct quantitative measurements of the fiber orientation on its surface. Fusion of a 3D

dense point cloud and thermal data was performed to enable the correct assessment of the fiber orientation in different regions of the complex shaped part without the distortion caused by the depth when one uses only the 2D information due to the geometric nature of the inspected part. A comparison between the results obtained with the proposed 3D/infrared merge approach and the results obtained using just the 2D information was presented in Figure 10.

Different tested regions (Figure 7) and respective results presented in Figure 9 and Table 2 show that the 3D information combined with the thermal information allow the fiber orientation measurement on complex 3D parts with only one field of view, i.e. with no need to reposition the part or the camera between two experiments for two different points. For example, Point A and Point C show accurate results of points where the camera's angle of incidence is almost 45° in modulus. Measurements on regions where there is an abrupt change on the surface geometric nature, e.g. edges (Point E and Point G) and corners (Point F), are also possible.

Nevertheless, it is possible to extend this work to use two thermal image sequences from two cameras in order to increase the surface of the part that could be inspected during one experiment. Additionally, this work can be applied to other thermography experiments. Once the camera(s) parameters are known and the identification of at least four points in the infrared sequence and the 3D dense point cloud is possible (so the POSIT algorithm can be applied), the merge of the infrared data and the 3D dense point cloud is straightforward. The thermal 3D model can provide more quantitative assessments of the part than the 2D infrared sequence alone.

Acknowledments

The authors would like to gratefully acknowledge support provided by the Canada Research Chair in Multipolar Infrared Vision (MiViM) and the industrial partners: Bell Helicopter Textron Canada Limited, Bombardier Inc., Pratt and Whitney Canada Corp., Avior Integrated Products Inc., Delastek Inc. and Hutchinson Inc. Canada. The authors would also like to acknowledge the support of the following agencies: CNPq, National Council for Scientific and Technological Development - Brazil; NSERC, Natural Sciences and Engineering Research Council of Canada; FQRNT, Quebec Fund for Research on Nature and Technology and CRIAQ, Consortium for Research and Innovation in Aerospace in Quebec. The parts tested in this work were manufactured in the Structures and Composites Materials Laboratory of McGill University and the thermography and 3D experiments were conducted in the Computer Vision and Systems Laboratory of Laval University.

References

[1] Maldague X. Theory and practice of infrared technology for nondestructive testing. 1^{st} ed. New York: Wiley-Interscience; 2001.

[2] De Senarmont MH. Mémoire sur la conductivité des substances cristallisées pour la chaleur: second mémoire. In: Annales de Chimie Physique; Vol. 3; 1848. p. 179–211.

[3] Krapez JC. Thermal ellipsometry applied to the evaluation of fibre orientation in composite. Tiré à part- Office national d'études et de recherches aerospatiales. 1994;(171):26.

[4] Krapez JC. Thermal ellipsometry: A tool applied for in-depth resolved characterization of fibre orientation in composites. In: Thompson DO, Chimenti DE, editors. Review of progress in quantitative nondestructive evaluation. Springer US; 1996. p. 533–540.

[5] Krapez JC, Gardette G, Balageas D. Thermal ellipsometry in steady-state and by lock-

in thermography. Application to anisotropic materials characterization. In: Balageas D, Busse G, Carlomagno G, editors. Proceedings of the QIRT 96; 1996. p. 267–262.

[6] Krapez JC, Gardette G. Characterisation of anisotropic materials by steady-state and modulated thermal ellipsometry. High Temperatures - High Pressures. 1998;30(5):567–574.

[7] Aindow J, Markham M, Puttick K, Rider J, Rudman M. Fibre orientation detection in injection-moulded carbon fibre reinforced components by thermography and ultrasonics. NDT international. 1986;19(1):24–29.

[8] Cielo P, Maldague X, Krapez JC, Lewak R. Optics-based techniques for the characterization of composites and ceramics. In: Bussiere JF, Monchalin JP, Ruud CO, Green Jr RE, editors. Nondestructive characterization of material handbook of technical diagnostics. Plenum Press; 1987. p. 733–744.

[9] Fernandes HC, Maldague X. Fiber orientation assessment on surface and beneath surface of carbon fiber reinforced composites using active infrared thermography. In: Proc. SPIE 9105, Thermosense: Thermal Infrared Applications XXXVI; Vol. 9105. International Society for Optics and Photonics; 2014. p. 91050D–91050D–9.

[10] Karpen W, Wu D, Steegmuller R, Busse G. Depth profiling of orientation in laminates with local lock-in thermography. In: Balageas D, Busse G, Carlomagno G, editors. Proceedings of the QIRT 94; 1994. p. 281–286.

[11] Karpen W, Wu D, Busse G. A theoretical model for the measurement of fiber orientation with thermal waves. Research in nondestructive evaluation. 1999;11(4):179–197.

[12] Fernandes HC, Maldague X. Fiber orientation assessment in carbon fiber reinforced composites using infrared thermography. In: Hoa SV, Hubert P, editors. Proc. 19th International Conference on Composite Materials (Montreal, Canada, July 2013); Vol. 1; 2013. p. 4970–4977.

[13] $Creaform^{©}$. Go!scan 3D scanner. 2014; Available from: http://www.goscan3d.com/en.

[14] Forsyth DA, Ponce J. Computer vision: A modern approach. 1^{st} ed. New Jersy: Prentice Hall Professional Technical Reference; 2002.

[15] Ju X, Nebel JC, Siebert JP. 3D thermography imaging standardization technique for inflammation diagnosis. In: Proc. SPIE 5640, Infrared Components and Their Applications. International Society for Optics and Photonics; 2005. p. 266–273.

[16] Barone S, Paoli A, Razionale A. A biomedical application combining visible and thermal 3D imaging. In: XVIII Congreso internactional de Ingenieria Grafica, Barcelona; 2006. p. 1–9.

[17] Bouguet JY. Complete camera calibration toolbox for Matlab®. December 2013; Available from: http://www.vision.caltech.edu/bouguetj/calib_doc.

[18] David P, Dementhon D, Duraiswami R, Samet H. Softposit: Simultaneous pose and correspondence determination. International Journal of Computer Vision. 2004;59(3):259–284.

[19] Dementhon D. Posit algorithm implementation: Softposit v. 0.9 (Matlab®). 2003; Available from: http://www.cfar.umd.edu/∼daniel/Site_2/Code.html.

[20] MathWorks. Measure properties of image regions - Matlab® regionprops. 2015; Available from: http://www.mathworks.com/help/images/ref/regionprops.html.

[21] Ageorges C, Ye L, Mai YW, Hou M. Characteristics of resistance welding of lap shear coupons. Part I: Heat transfer. Composites Part A: Applied Science and Manufacturing. 1998;29(8):899–909.